applied sciences

MDPI

Article

# Numerical Descriptions of Hot Flow Behaviors across β Transus for as-Forged Ti–10V–2Fe–3Al Alloy by LHS-SVR and GA-SVR and Improvement in Forming Simulation Accuracy

**Guo-Zheng Quan [1,*], Zhi-Hua Zhang [1], Le Zhang [1] and Qing Liu [2]**

[1] State Key Laboratory of Mechanical Transmission, School of Material Science and Engineering, Chongqing University, Chongqing 400044, China; zhihuazhang66@126.com (Z.-H.Z.); lezhang163@163.com (L.Z.)

[2] China National Erzhong Group Co., Deyang 618000, Sichuan, China; liuqing8396@163.com

* Correspondence: quangz3000@sina.com; Tel./Fax: +86-023-6511-1493

Academic Editor: Stanislaw M. Dubiel
Received: 12 June 2016; Accepted: 22 July 2016; Published: 27 July 2016

**Abstract:** Hot compression tests of as-forged Ti–10V–2Fe–3Al alloy in a wide temperature range of 948–1123 K and a strain rate range of 0.001–10 $s^{-1}$ were conducted by a servo-hydraulic and computer-controlled Gleeble-3500 machine. In order to accurately and effectively model the non-linear flow behaviors, support vector regression (SVR), as a machine learning method, was combined with Latin hypercube sampling (LHS) and genetic algorithm (GA) to respectively characterize the flow behaviors, namely LHS-SVR and GA-SVR. The significant characters of LHS-SVR and GA-SVR are that they, with identical training parameters, can maintain training accuracy and prediction accuracy at stable levels in different attempts. The study abilities, generalization abilities and modelling efficiencies of the mathematical regression model, artificial neural network (ANN), LHS-SVR and GA-SVR were compared in detail by using standard statistical parameters. After comparisons, the study abilities and generalization abilities of these models were shown as follows in ascending order: the mathematical regression model < ANN < GA-SVR < LHS-SVR. The modeling efficiencies of these models were shown as follows in ascending order: mathematical regression model < ANN < LHS-SVR < GA-SVR. The flow behaviors outside experimental conditions were predicted by the well-trained LHS-SVR, which improves the simulation precision of the load-stroke curve.

**Keywords:** titanium alloy; flow stress; constitutive model; support vector regression; Latin hypercube sampling; genetic algorithm

## 1. Introduction

Ti–10V–2Fe–3Al alloy, a typical near-β titanium alloy, has the advantages of high strength, good toughness, excellent stress-corrosion resistance, etc., so it was widely utilized for key structural parts in the aerospace industry. It is universally acknowledged that stress-strain data play important roles in many areas, for instances speculating work hardening (WH) and dynamic recovery (DRV) [1], characterizing dynamic recrystallization evolution [2], improving processing maps [3], etc. A precise model of flow behaviors is critical to reflect material properties and investigate microscopic deformation mechanisms. The pre-existing literature demonstrates that there are close relationships among flow stress, strain, strain rate and temperature. Therefore, it is important to construct and further accurately predict the highly non-linear flow behaviors of materials.

Nowadays, there exist three representative models in characterizing flow behaviors of metals, i.e., the empirical/semiempirical model, the analytical model and the phenomenological model [4–6]. Hollomon presented a typical empirical model ($\sigma = K_H \varepsilon^n$) for plastic deformation with a lower level of accuracy, in which $K_H$ and $n$ are constants [7]. Afterwards, Guan et al. [8] proposed an improved empirical model with a higher level of accuracy (correlation coefficient $R$ = 0.998) due to considering the effects of strain rate and strain on stress. However, the empirical model cannot accurately track the highly non-linear flow behaviors at different strain rates and temperatures. Additionally, many parameters of the empirical model need to be recalculated when some new experimental data are involved. The analytical model requires explicit and thorough study of microscopic deformation mechanisms, such as dislocation theory, DRV, DRX, etc. [9]. Vanini et al. established an analytical model ($R \approx 0.988$), which just considered the phase mixture law and boundary layer characteristics of the hot deformation behaviors of functionally-graded steels [10]. George Z. Voyiadjis et al. established the analytical constitutive models involving dislocations interaction mechanisms and thermal activation energy for the flow behaviors under different temperatures and strain rates of face centered cubic (FCC) and body centered cubic (BCC) metals [11]. In the investigation of George Z. Voyiadjis et al., the mobile dislocation density has different influences on flow behaviors at different temperatures and strain rates, so it needs to establish several constitutive models at different deformation conditions; otherwise, the physical-based analytical model cannot accurately characterize the highly non-linear deformation behaviors [11]. Besides, analytical models need many precise experiment data to construct a mathematical model of complicated microscopic deformation mechanisms. Thereby, analytical models have not been widely utilized in characterizing intricate flow behaviors of metals.

The phenomenological model involves the mathematical regression equation and intelligence algorithm, and it does not need to deeply investigate complicated microscopic deformation mechanisms. The mathematical regression equations just need to calculate some essential material constants and further be fitted based on limited experimental data. At present, the typical Arrhenius-type equation of the phenomenological model and its modified forms were used to characterize the hot flow behaviors of many materials, such as Ti60 ($R \approx 0.99$) [12], Ti–6Al–4V [13], pure titanium [14], etc. Other phenomenological models involve the representative Johnson–Cook model ($R$ = 0.9772), the Fields–Backofen model ($R$ = 0.87025), the Khan–Huang–Liang model ($R$ = 0.96559), the mechanical threshold stress model ($R$ = 0.9614), etc.; nevertheless, they have large fluctuant accuracies at different strain rates and temperatures [15]. Additionally, Akbari et al. further pointed out that the original Johnson–Cook model was not able to predict the softening part of the flow stress curves [16]. The mathematical regression equations of the phenomenological model cannot accurately track the highly non-linear flow behaviors at different strain rates and temperatures [15,17]. Because they are mathematically fitted based on limited experimental data. lately, the artificial neural network (ANN) of intelligence algorithm, which imitates biological neural systems, was adopted to characterize the flow behaviors of AZ80 magnesium alloy [18], A356 aluminum alloy [19], Ti–10V–2Fe–3Al alloy [20], etc. ANN needs to try many network topologies and training parameters to achieve a higher accuracy, which will consume much time. For a certain dataset, the identical network topology and training parameters of an ANN will obtain fluctuant accuracies in different attempts. ANN can meet network topology and training parameters well to achieve a higher accuracy level; however, these accurate results have poor reproducibility. Worse still, ANN easily falls into local extreme values and cannot attain a globally-optimal solution.

Support vector regression (SVR), as a machine learning method according to the structural risk minimization principle and statistical learning theory, is mostly used in the regression analysis field [21]. SVR has the advantages of strong generalization ability, robustness and a systemic theoretical system. Compared to ANN, SVR can avoid falling into local extreme values and can attain a globally-optimal solution. For a certain dataset, an SVR with identical training parameters will maintain training accuracy and prediction accuracy at stable levels in different attempts. In this work, SVR was adopted to characterize the hot flow behaviors of as-forged Ti–10V–2Fe–3Al alloy on account of

its excellent advantages. The learning ability and generalization ability of an SVR rely on three parameters (penalty factor $C$, kernel parameter $\gamma$ and insensitive loss function $\zeta$), especially the mutual impacts among them. Therefore, SVR needs to adjust the three parameters ($C$, $\gamma$ and $\zeta$) to attain a precise prediction model. An SVR with appropriate parameters $C$, $\gamma$ and $\zeta$ will accurately study the stress-strain curves and appropriately ignore some singular points of stress-strain data to accord with the overall trend of the curves. The influence of the combination of the three parameters ($C$, $\gamma$ and $\zeta$) on the learning ability and generalization ability of an SVR should be synthetically considered. It is time consuming to independently adjust the three parameters one by one to establish an SVR that can accurately characterize the hot flow behaviors of as-forged Ti–10V–2Fe–3Al alloy. Thereby, it is important to find a stable and efficient method to realize the optimal selection of the three parameters in SVR. Lou et al. established an SVR combined with particle swarm optimization (PSO) to characterize the flow behaviors of AZ80 magnesium alloy in which PSO was adopted to select the parameters $C$, $\gamma$ and $\zeta$, and this study indicates that the model is more accurate than ANN and the constitutive equation; besides, the sample dependence of the SVR is lower [22]. Raghuram Karthik Desu et al. constructed an SVR to characterize the flow behaviors of Austenitic Stainless Steel 304, and they found that SVR is more precise, efficient and reliable than the mathematical regression equations, such as the revised-Arrhenius model, the Johnson–Cook model, the revised Zerrili–Armstrong model and the intelligence algorithm ANN model [23]. The best correlation coefficient ($R$) in the work of Raghuram Karthik Desu et al. is 0.9989 at a high accuracy level; nevertheless, they only attempted a few parameter combinations of the three parameters ($C$, $\gamma$ and $\zeta$), and there is still room for improvement in accuracy and efficiency [23].

The Latin hypercube sampling (LHS) method, as a uniform sampling method, was used to ensure that sampling areas can be uniformly covered by all sampling points [24]. In this work, the sampling points represent the combinations of the three parameters ($C$, $\gamma$ and $\zeta$) in three-dimensional space. There are two advantages of LHS. Firstly, the sampling points generated by LHS can effectively fill the sampling space. Secondly, less sampling points generated by LHS can represent more combinations of parameters. In this work, a novel SVR for the flow behaviors of as-forged Ti–10V–2Fe–3Al alloy combined with LHS was established, i.e., the LHS-SVR. Compared to the work of Raghuram Karthik Desu et al. [23] the sampling points generated by LHS-SVR can effectively fill the sampling space and represent more combinations of the three parameters ($C$, $\gamma$ and $\zeta$). LHS-SVR can show the influences of the three parameter combinations on the accuracy of the model, and this influence law can be used as a reference to researchers when they need to select the three parameters. However, LHS-SVR needs to calculate the many parameter combinations in the search space, and there is still room for improvement in efficiency.

GA, as a global optimization algorithm, has been widely used in the multi-parameter optimization area on account of the advantages of parallel processing, high efficiency and strong robustness. GA searches the optimal parameters in the solution space by imitating the natural selection process and genetic mechanism. In order to use the advantages of GA, an SVR model of the hot flow behaviors of as-forged Ti–10V–2Fe–3Al alloy combined with GA was constructed, i.e., the GA-SVR. In GA-SVR, GA was utilized to efficiently seek the optimal parameter combination of the three parameters ($C$, $\gamma$ and $\zeta$). The GA-SVR only requires representative training samples from the research problem and then self-adaptively and dynamically adjusts the three parameters ($C$, $\gamma$ and $\zeta$) to attain the most accurate SVR.

In this work, the comparisons of the learning abilities, generalization abilities and modelling efficiencies of the mathematical regression model, ANN, LHS-SVR and GA-SVR were investigated. A standard statistical parameter, average absolute relative error (*AARE*), was utilized to estimate the predicted performance of these four prediction models. In the comparisons of study abilities, the LHS-SVR and GA-SVR have larger $R$-values and lower *AARE*-values, which show that the LHS-SVR and GA-SVR can sufficiently and accurately learn the training samples. The study abilities of these models were shown as follows in ascending order: ANN < GA-SVR < LHS-SVR. In the comparisons of

the generalization abilities, the LHS-SVR and GA-SVR have larger *R*-values and lower *AARE*-values, which indicate that the LHS-SVR and GA-SVR can accurately predict the highly non-linear flow behaviors. The generalization abilities of these four models were shown as follows in ascending order: the mathematical regression model < ANN < GA-SVR < LHS-SVR. ANN can meet well the network topology and training parameters to achieve a higher accuracy level; nevertheless, these accurate results have poor reproducibility. The significant character of SVR is that an SVR with identical training parameters will maintain training accuracy and prediction accuracy at stable levels in different attempts for a certain dataset. Besides, the *R*-values between the training samples and fitted values of LHS-SVR and GA-SVR of the Ti–10V–2Fe–3Al alloy are larger than 0.9999, showing that the fitting precisions of LHS-SVR and GA-SVR are larger than the empirical/semiempirical model and the analytical model. The computing time of a training process of LHS-SVR is greatly shorter than ANN. Compared to ANN and the method that manually adjusts the three parameters one by one to obtain an accurate prediction model, the intelligence algorithm LHS-SVR can automatically calculate the parameter combinations one by one in the search space to find the optimal value, which improves the computational efficiency to a certain extent. Based on the selection, crossover and mutation operators, the GA-SVR can self-adaptively and dynamically adjust the processes of selection, crossover and mutation and rapidly generate optimal results, which greatly improves the computational efficiency compared to LHS-SVR and ANN. After comparisons, the modeling efficiencies of these models were shown as follows in ascending order: the mathematical regression model < ANN < LHS-SVR < GA-SVR. Besides, LHS-SVR and GA-SVR only need representative training samples from the research and then automatically adjust the three parameters $C$, $\gamma$ and $\zeta$ to obtain the accurate SVR. The modeling efficiencies of LHS-SVR and GA-SVR are higher than the empirical/semiempirical model and the analytical model. In finite element software, if the software needs to invoke stress-strain data, which are not beforehand inputted into the software, it mainly calculates unknown stress-strain data by mathematical interpolation means. However, hot flow behaviors of materials at different conditions (such as different strain rates and temperatures) are highly non-linear and complicated. The mathematical interpolation method cannot correctly predict the hot flow behaviors of materials and will obtain inaccurate simulation results. The stresses outside experimental conditions were predicted by the well-trained LHS-SVR, which enhances the simulation precision of the load-stroke curve and can further improve the related research fields where stress-strain data play important roles.

## 2. Acquisition of Experimental Stress-Strain Data

The chemical compositions (wt %) of as-forged Ti–10V–2Fe–3Al alloy are as follows: V–10, Al–3.0, Fe–1.9, O–0.13, Si–0.05, C–0.05, N–0.05, H–0.0125, Ti (balance). The original as-forged Ti–10V–2Fe–3Al alloy was supplied in the form of bar with a diameter of 180 mm. The homogenized metal bar of Ti–10V–2Fe–3Al alloy was machined by wire-electrode cutting into several specimens with a height of 12 mm and a diameter of 10 mm, and the cylinder axes of these specimens are parallel to the axial line of the original bar. Figure 1 shows the optical microstructure of the original as-forged Ti–10V–2Fe–3Al alloy, in which the tiny acicular α-phase grains dispersively distribute in the matrix of large β-phase grains. The transformation temperature from the (α + β) phase to the β-phase of the alloy is about 1068 ± 5 K. All of the specimens were homogenized under a temperature of 1033 K for 60 min. These specimens were compressed on a servo-hydraulic and computer-controlled Gleeble-3500 machine Dynamic Systems Inc., New York, NY, USA). The test samples were heated at a rate of 10 K/s and held at a certain temperature for 150 s to assure a uniform temperature and to reduce material anisotropism. The test samples were compressed with a height reduction of 60% (true strain 0.9) at the strain rates of 0.001, 0.01, 0.1, 1 and 10 $s^{-1}$ and the temperatures of 948, 973, 998, 1023, 1048, 1073 , 1098 and 1123 K, and then, these deformed test samples were rapidly quenched into water to retain the microstructures acquired at high temperatures.

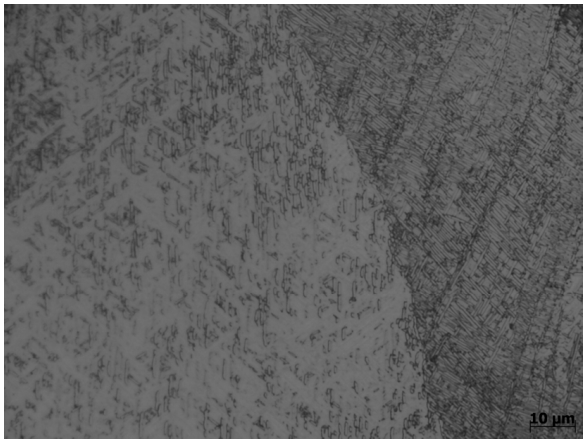


**Figure 1.** Optical photograph of the original as-forged Ti–10V–2Fe–3Al alloy.

Figure 2 shows the experimental compressive stress-strain curves of as-forged Ti–10V–2Fe–3Al alloy at different strain rates and temperatures. The variation of stresses with strain can be summarily classified into three stages. At the first stage, the stress quickly increases to a critical value with the increase of strain, where work hardening (WH) dominates this stage; at the same time, the stored energy in grain boundaries increases rapidly to the activation energy of dynamic recrystallization (DRX). At the second stage, DRX and dynamic recovery (DRV) occur and further grow, and the increasing rate of flow stress declines until a maximum stress where the thermal softening begins to exceed WH on account of DRX and DRV. The changes of stresses exhibit two types at the final stage: in the ($\alpha$ + $\beta$) phase, the flow stress continuously declines with distinct DRX softening (948–1023 K and 0.001–0.1 $s^{-1}$) [25]; the flow stress approximately maintains at a stable level where the $\beta$-phase predominates (1048–1123 K and 0.001–0.1 $s^{-1}$), which indicates a new dynamic balance between WH and DRV [25]. The pre-existing literature demonstrates that there are close relationships among flow stress, strain, strain rate and temperature. It is well known that stress-strain data play important roles in many areas, for instances speculating about WH and DRV [1], improving processing maps [3], characterizing dynamic recrystallization evolution [2], etc. A precise model of flow behaviors is critical to reflect material properties and to improve numerical simulation precision [26]. Thereby, it is important to establish a model to accurately characterize the highly non-linear flow behaviors.

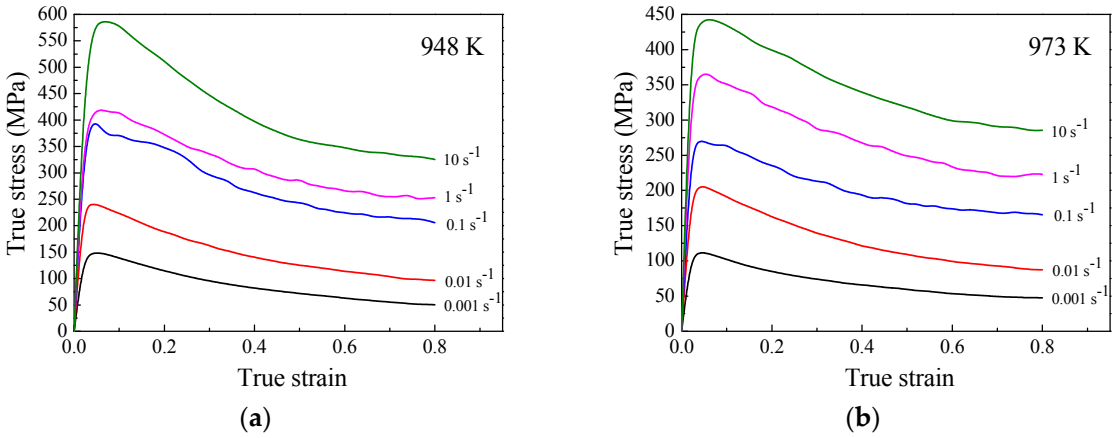


**Figure 2.** *Cont.*

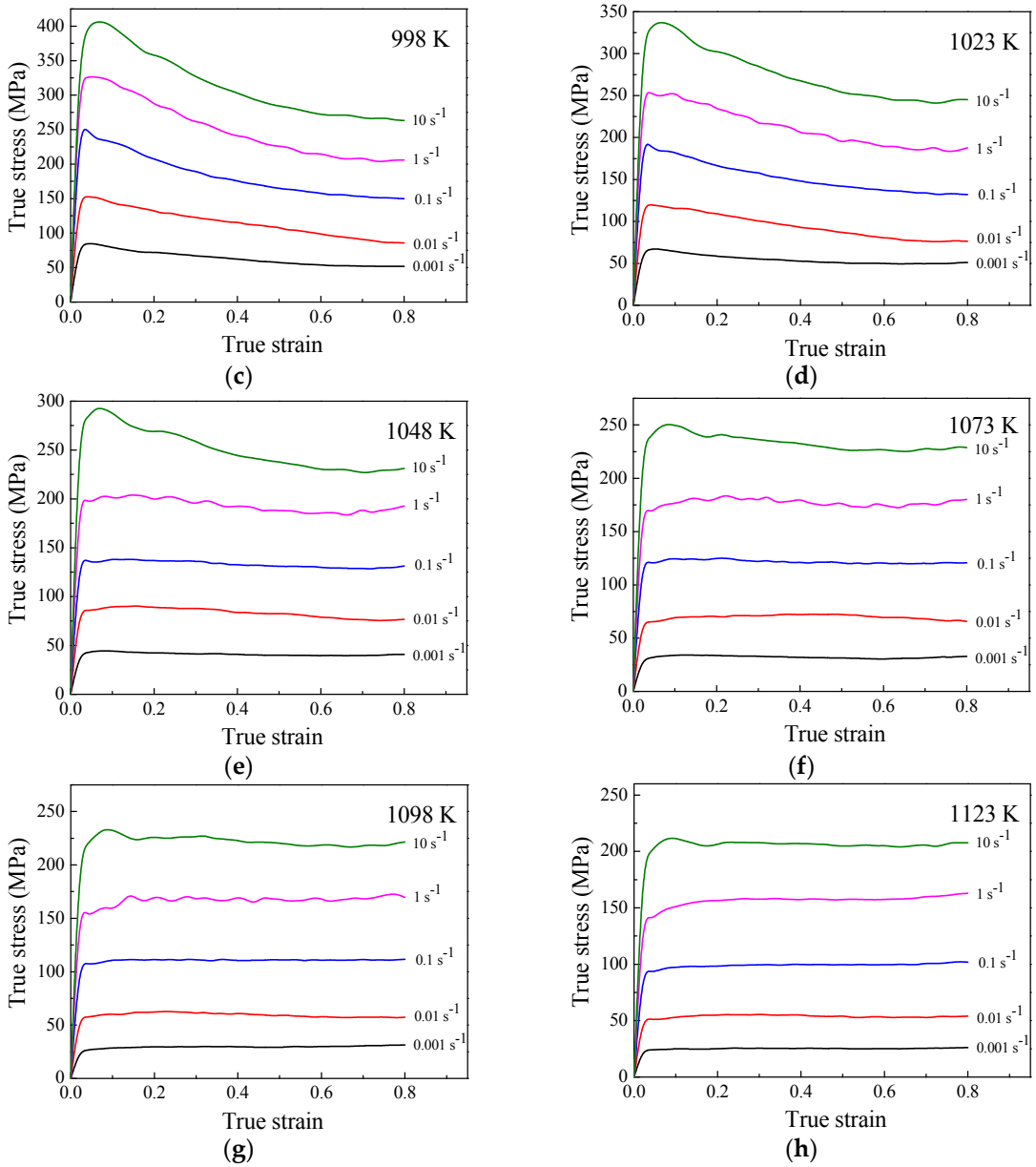


**Figure 2.** True stress-strain curves of the Ti–10V–2Fe–3Al alloy at different strain rates and temperatures: (**a**) 948 K; (**b**) 973 K; (**c**) 998 K; (**d**) 1023 K; (**e**) 1048 K; (**f**) 1073 K; (**g**) 1098 K; (**h**) 1123 K.

## 3. Development of Support Vector Regression for the Hot Flow Behaviors of as-Forged Ti–10V–2Fe–3Al Alloy

In this study, support vector regression (SVR) was used to establish a model to characterize the flow behaviors of as-forged Ti–10V–2Fe–3Al alloy on account of its excellent advantages of regression analysis ability, robustness and high efficiency.

### *3.1. The Basic Principles of SVR*

Support vector machine (SVM) is a machine learning method according to the structural risk minimization principle and statistical learning theory [21]. SVM is primarily used for regression analysis and classification, so it is classified into support vector regression (SVR) and support vector classification (SVC). In SVR, linearly-inseparable low-dimensional data are mapped into linearly-separable multidimensional data by using the kernel function.

SVR has several advantages as follows: firstly, in SVR, linearly-inseparable low-dimensional data are mapped into linearly-separable high-dimensional data by using the kernel function, and this mapping can be briefly expressed by Equation (1). With the help of the kernel function, SVR can avoid the curse of dimensionality and construct the linear discriminant function in high dimensional space to implement the nonlinear discrimination in the original space. Secondly, comparing SVR to artificial neural network (ANN), the computational process of SVR is robust, and SVR will obtain the globally-optimal solution; while ANN easily falls into local extreme values. SVR has a complete theoretical basis and strong generalization ability, and it does not need to try many network topologies to achieve a high accuracy level.

$$x \to \Phi(x) = (g_1\Phi_1(x), g_2\Phi_2(x), \ \dots, g_n\Phi_n(x)) \quad g_n \in R, \Phi_n \in R \tag{1}$$

where $x$ is the input variable; $\Phi(x)$ is the mapping function; $g_1$, $g_2$, ... , $g_n$ are constants.

An SVR equipped with the radial basis function (RBF) expressed by Equation (2) can achieve a higher regression accuracy. Therefore, the RBF was adopted in this work.

$$k(x_i, x) = \exp(-\gamma \,||\, x_i - x \,||^2), \gamma = \frac{1}{2\tau^2} \tag{2}$$

where $\gamma$ and $\tau^2$ are variable parameters of the RBF. A suitable parameter $\tau^2$ will avoid over-fitting and under-fitting of data in SVR.

It is assumed that the original data are $(x_1, y_1), (x_2, y_2), (x_3, y_3), \ \dots, (x_i, y_i), \ \dots, (x_l, y_l), x_i, y_i \in R$, and the function $f(x)$ is able to estimate all data. In SVR, the $y = f(x)$ can be expressed by Equation (3):

$$f(x) = \boldsymbol{\omega} \cdot \boldsymbol{x} + b \tag{3}$$

where $\boldsymbol{\omega}$ is a multidimensional column vector; $b$ is a bias term. Additionally, the optimal function can be expressed as:

$$\min \frac{1}{2} \,||\, \boldsymbol{\omega} \,||^2 + C\sum_{i=1}^{l} (\xi_\iota + \xi_i{}^*) \tag{4}$$

s.t.

$$\begin{cases} y_i - \boldsymbol{\omega} \cdot x_i - b \leqslant \zeta + \xi_i \\ \boldsymbol{\omega} \cdot x_i + b - y_i \leqslant \zeta + \xi_i{}^* \\ \xi_\iota, \xi_\iota{}^* \geqslant 0 \end{cases} \tag{5}$$

where $\boldsymbol{\omega}$ is a multidimensional column vector; $C$ is a penalty factor; $\xi_\iota$ and $\xi_\iota{}^*$ are slack variables, which can improve regression accuracy; $\zeta$ is an insensitive loss function, which greatly impacts the regression accuracy of SVR. In this work, the input variables $x$ of SVR include strain ($\varepsilon$), strain rate ($\dot{\varepsilon}$) and temperature ($T$), and the target output $f(x)$ is the flow stress ($\sigma$) of as-forged Ti–10V–2Fe–3Al alloy.

The regression function in SVR can be expressed by Equation (6):

$$f(x) = \sum_{i\,=\,1}^{l} (\alpha_i - \alpha_i{}^*) k(x_i, x) + b \tag{6}$$

where $\alpha_i$ is the Lagrange multiplier; $k(x_i, x)$ is a kernel function; $b$ is a bias term.

### *3.2. The Influence of Parameters Selection on the Performance of SVR*

In SVR, the learning ability and generalization ability can be improved by appropriate parameters settings, and such parameters are penalty factor $C$, kernel parameter $\gamma$ and non-sensitive loss function $\zeta$.

(1) Penalty factor $C$

The robustness and complexity of SVR are influenced by the penalty factor $C$. A larger $C$-value in SVR indicates that all data samples are important and each sample should be correctly fitted, which will cause the SVR to be complicated and over-fitted; whereas a smaller $C$-value in SVR indicates that some singular points can be ignored. However, the phenomenon of under-fitting will occur in SVR when the $C$-value is too small.

(2) The parameter $\gamma$ of the basis kernel function (RBF)

The parameter $\tau^2$ expressed by Equation (2) determines the data mapping process and even influences the learning ability and generalization ability of the model. The phenomenon of over-fitting will occur in the following cases: (a) $C$-value is set as a certain value and $\tau^2 \to 0$; (b) $\tau^2$ is set as a certain value and $C \to \infty$ [27]. Additionally, the phenomenon of under-fitting will occur in the following cases: (a) $C$ is set as a smaller value and $\tau^2 \to 0$; (b) $C$ is set as a certain value and $\tau^2 \to \infty$; (c) $\tau^2$ is set as a certain value and $C \to 0$ [27].

(3) The non-sensitive loss function $\zeta$

In SVR, the $\zeta$-value influences the number of support vectors and further influences the regression accuracy of the model.

It can be concluded that the learning ability and generalization ability of SVR rely on the three parameters $C$, $\gamma$ and $\zeta$, especially the mutual impacts among them. An SVR with appropriate parameters $C$, $\gamma$ and $\zeta$ will accurately study the stress-strain curves and appropriately ignore some singular points of stress-strain data to accord with the overall trend of the stress-strain curves. In SVR, it is time consuming to independently optimize each parameter. The influence of the combination of the three parameters ($C$, $\gamma$ and $\zeta$) on the learning ability and generalization ability of SVR should be synthetically considered. It is inefficient to manually adjust the three parameters one by one to establish an SVR that can accurately characterize the hot flow behaviors of as-forged Ti–10V–2Fe–3Al alloy. Thereby, it is important to find a stable and efficient method to realize the optimal selection of the three parameters in SVR.

### *3.3. The Prediction Model of Flow Behaviors Based on SVR and Latin Hypercube Sampling*

In this section, Latin hypercube sampling (LHS) was combined with SVR to characterize the hot flow behaviors of the Ti–10V–2Fe–3Al alloy, and the novel model was called LHS-SVR in this study.

#### 3.3.1. The Basic Principles of LHS

The LHS method, as a uniform sampling method, was used to ensure that sampling areas can be uniformly covered by all sampling points [24]. In this work, the sampling points represent the combinations of the three parameters ($C$, $\gamma$ and $\zeta$) in three-dimensional space. There are two advantages of LHS. Firstly, the sampling points generated by LHS can effectively fill the sampling space. Assuming that there is a sampling with two variables and nine levels, so there are $9 \times 9 = 81$ sampling points in the sampling space. With the help of the LHS method, only nine points that uniformly cover the sampling space need to be investigated, as shown in Figure 3. The research efficiency is greatly improved by LHS. Secondly, the less sampling points generated by LHS can represent more combinations of parameters. Assuming that there is a sampling with two variables and nine levels. As shown in Figure 3, all levels of each factor are considered by using LHS, while only three levels of each factor are investigated by using the orthogonal test.

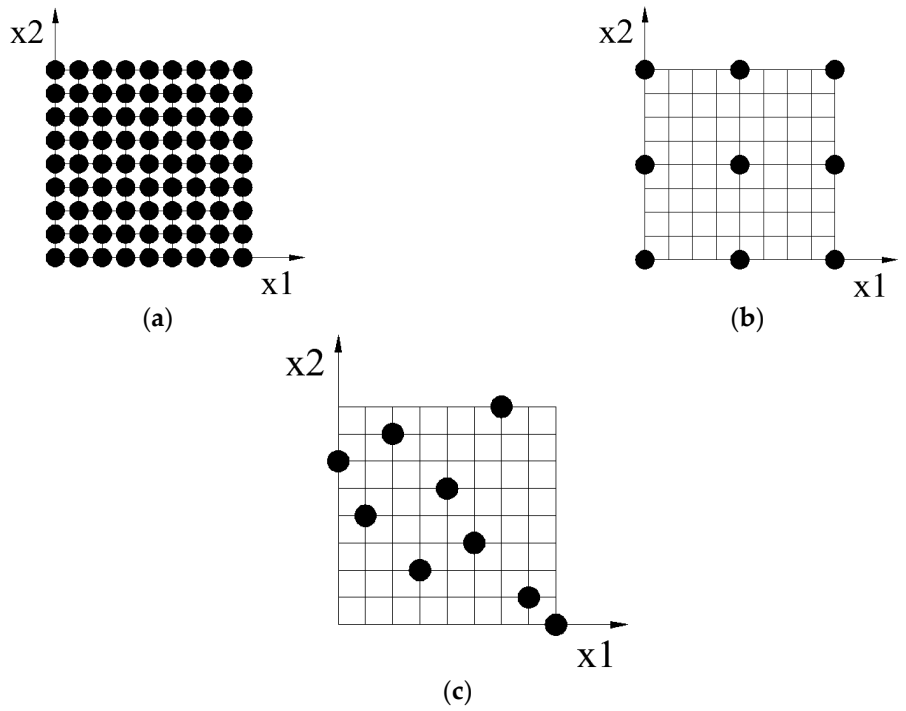


**Figure 3.** The sketch maps of: (**a**) all sampling points; (**b**) the sampling points designed by the orthogonal test; and (**c**) the sampling points generated by Latin hypercube sampling (LHS).

3.3.2. The Establishment of the Prediction Model LHS-SVR for the Flow Behaviors

In this work, 1520 input-output pairs were selected from the stress-strain curves to train and test the LHS-SVR. Among the 1520 input-output pairs, 21.05% (320) of stress points at the strain range of 0.1–0.8 with a distance of 0.1 were not utilized for training, but for testing the generalization ability of the developed LHS-SVR, and the remaining datasets were adopted to train the LHS-SVR. The cross-validation method, as an effective means of evaluating the accuracy of machine learning, was used in this investigation to evaluate the accuracy of the established LHS-SVR. In the cross-validation method, the original data are divided into $N$ datasets. Each separate dataset is alternately retained as validation data, and the other ($N$-1) datasets are used to train the LHS-SVR. The performance of the LHS-SVR is evaluated by the average number of an evaluation index in an $N$ validation process. Here, the number $N$ was set as five. Additionally, an evaluation index mean square error (*MSE*) expressed by Equation (7) between training stress data and validation stress data was introduced to evaluate the performance of the LHS-SVR.

$$MSE = \frac{1}{N}\sum_{i=1}^{N}[f(x_i) - y_i]^2 \tag{7}$$

where $f(x_i)$ is the predicted stress data; $y_i$ is the experimental stress data. Additionally, $N$ is equal to the number of stress-strain samples.

In addition, another evaluation index correlation coefficient ($R$) expressed as Equation (8) was used to estimate the degree of correlation between the experimental flow stresses and predicted flow stresses [28]. A larger $R$-value near one demonstrates a good correlation between the two variables, and vice versa.

$$R = \frac{\sum_{i=1}^{N}(E_i - \overline{E})(P_i - \overline{P})}{\sqrt{\sum_{i=1}^{N}(E_i - \overline{E})^2 \sum_{i=1}^{N}(P_i - \overline{P})^2}} \tag{8}$$

where $E$ is the sample of experimental stress-strain values; $P$ is the sample of predicted stress-strain values; $N$ is equal to the number of samples.

Assuming that there is an $n$-dimension sampling space; $x_i$ is the $i$-th dimension variable, $i = 1, 2, ..., n$. $x_i \in [l_i, u_i]$; $l_i$ and $u_i$ are the boundary values of the $i$-th dimension variable. The sampling process of LHS-SVR, which selects $n_0$ sampling points, is as follows:

Step 1 Determine the searching sampling space and sample size $n_0$. The domain of definition $[l_i, u_i]$ of $x_i$ was uniformly divided into $n_0$ intervals. Then, the $n$-dimension space was divided into ${n_0}^n$ hypercubes. Generate an $n_0 \times n$ matrix, and each column of the matrix is a random permutation of {1, 2, 3, ..., $n_0$}. Each row of the matrix represents a selected hypercube. The central points of all selected hypercubes are the sampling points.

Step 2 The *MSE*-values of all sample points were calculated by the cross-validation method.

Step 3 Search the optimal parameter combination.

Step 4 Reset the searching sampling space; increase the searching sample size.

Step 5 Search the optimal parameter combination again.

Step 6 Output the optimal parameter combination.

The specific flowchart of the LHS-SVR is illustrated in Figure 4.

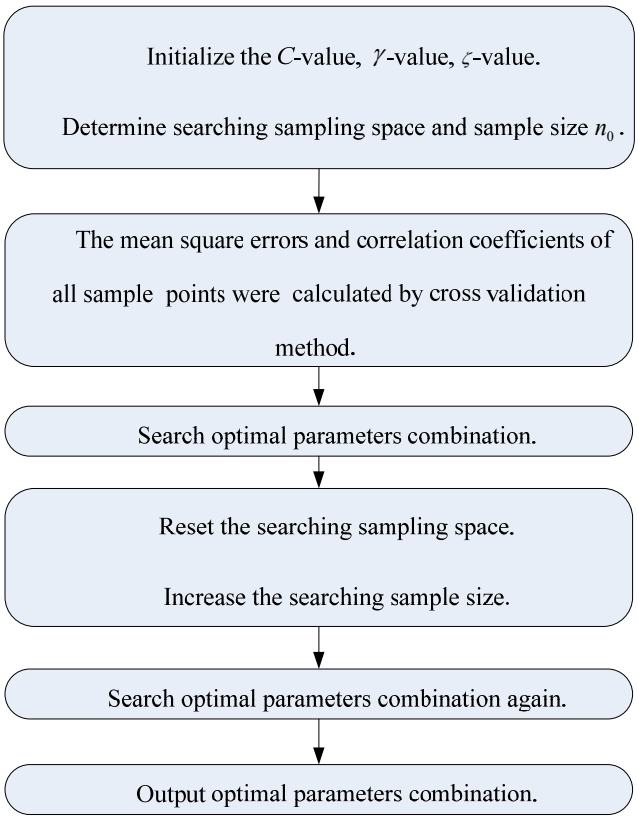


**Figure 4.** The specific flowchart of LHS-SVR.

In the preliminary search, 500 sample points were preset in the intervals: $C \in [0, 100]$, $\gamma \in [0, 100]$, $\zeta \in [0, 100]$; and the *MSE*-values and *R*-values of all samples were calculated. Each point represents a parameter combination. In the preliminary search, 50 points with larger *R*-values are illustrated in Figure 5a, so as to display the distribution of solutions in the search space. As shown in Figure 5a, the purple points with the *R*-values that are larger than 0.9990 are located in the following intervals: $C \in [0, 20]$, $\gamma \in [0, 20]$, $\zeta \in [0, 20]$; and the $C$, $\gamma$ and $\zeta$ of the best parameter combination

($R$ = 0.999750) are 11.9, 10.9 and 6.9, respectively. Therefore, the next search space should be reset in the intervals. In the second search, 50 points with larger $R$-values are also illustrated in Figure 5b. As shown in Figure 5b, most of the $R$-values of the parameter combination points in this interval are larger than 0.9998. Additionally, the $R$-values of few parameter combination points are larger than 0.9999, which meets the accuracy requirements, and the $C$, $\gamma$ and $\zeta$ of the best parameter combination ($R$ = 0.999997) are 14.7, 5.34 and 0.06, respectively. It can be summarized that the sampling points generated by the LHS-SVR can effectively fill the sampling space and represent more combinations of the parameters $C$, $\gamma$ and $\zeta$.

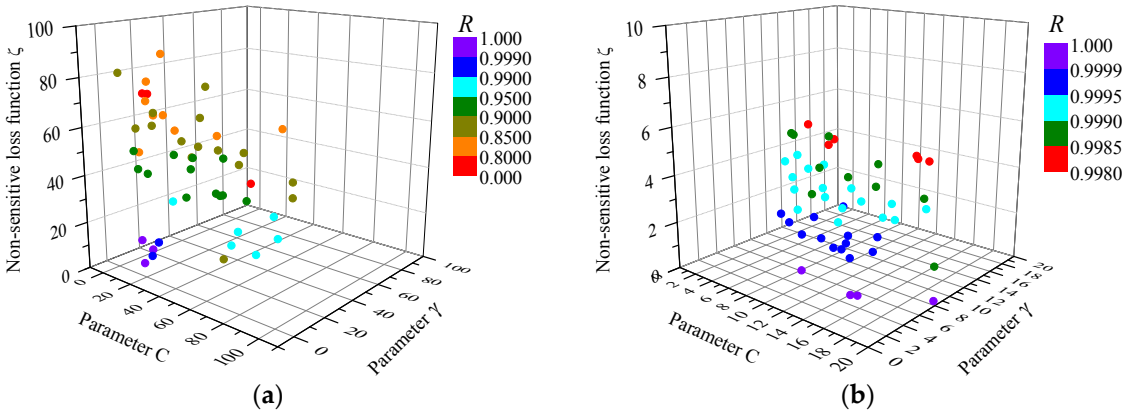


**Figure 5.** The distributions of $R$-values of the (**a**) preliminary searching result and (**b**) second searching result of the LHS-SVR.

### *3.4. The Prediction Model of Flow Behaviors Based on SVR and Genetic Algorithm*

The computing time of a training process of LHS-SVR is greatly shorter than ANN. However, LHS-SVR needs to calculate many parameter combinations in the search space, and there is still room for improvement in efficiency. In this section, genetic algorithm (GA) was combined with SVR to characterize the hot flow behaviors of the Ti–10V–2Fe–3Al alloy, and the model was called GA-SVR in this study. In GA-SVR, GA was used to efficiently seek the optimal parameter combination of the three parameters ($C$, $\gamma$ and $\zeta$).

#### 3.4.1. The Basic Principles of GA

GA, as a global optimization algorithm, has been widely used in multi-parameters optimization on account of its advantages of parallel processing, high efficiency and strong robustness. GA searches the optimal parameters in solution space by imitating the natural selection process and genetic mechanism. In GA, a population consists of some individuals that are encoded by gene encoding. The population was updated by the operators of selection, crossover and mutation. The selection operator (also known as the reproduction operator) is utilized in GA to select superior individuals and eliminate inferior individuals. According to the fitness value of each individual, an individual that has a higher fitness value is inherited to the next generation with a greater probability. The crossover operator in GA is used to exchange some genes between two paired chromosomes, so as to generate two new individuals. The crossover operator is the main method to generate new individuals, and it determines the global search ability of GA. The mutation operator in GA is utilized to change some of the values of the symbol string of individuals, so as to generate a new individual. The mutation operator is the auxiliary method to generate new individuals, and it determines the local search ability in GA. The crossover operator and mutation operator cooperate with each other to complete the global search and the local search in the search space. The individual fitness value of the population after iteration calculations will constantly come close to the optimal value.

3.4.2. The Establishment of Prediction Model GA-SVR for the Flow Behaviors

In order to utilize the advantages of strong robustness, high efficiency and parallel processing of GA, a prediction model of the deformation behaviors of the Ti–10V–2Fe–3Al alloy combined with GA and SVR was established, namely GA-SVR. The specific flowchart of GA-SVR is illustrated in Figure 6.

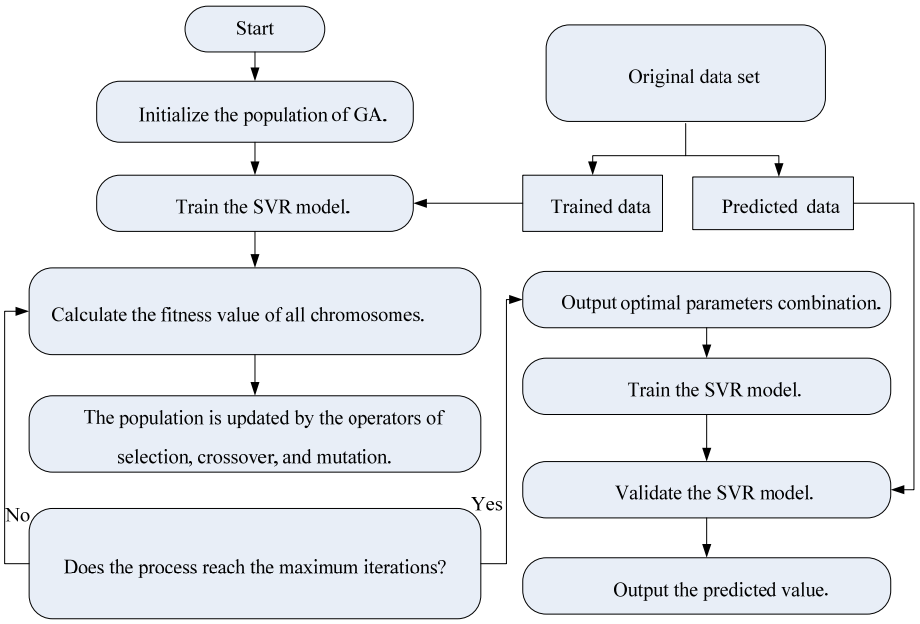


**Figure 6.** The specific flowchart of GA-SVR.

The detailed process of GA-SVR is as follows:

Step 1 Initialize the population of the GA-SVR. The parameters $C$, $\gamma$ and $\zeta$ were encoded to chromosomes of individuals. The population number was set as 20. The search space was preset in the intervals: $C \in [0, 100]$, $\gamma \in [0, 100]$, $\zeta \in [0, 100]$.

Step 2 The fitness values of all individuals were calculated by the fitness function expressed as Equation (7).

Step 3 The population was renewed by the operators of selection, crossover and mutation. The crossover probability $P_C$-value is usually set in the range of 0.6–0.9. A larger $P_C$ will rapidly generate new chromosomes in populations; nevertheless, it will increase the risk of premature convergence and lose excellent gene structure. A smaller $P_C$ will slow down the genetic evolution process. Here, the $P_C$-value was set as 0.75. The mutation operator determines the local searching ability of GA-SVR, so it should be set as a smaller value. Here, the $P_m$-value was set as 0.02. The cross-validation method was adopted to estimate the precision of GA-SVR.

Step 4 Stop criterion: The process of the GA-SVR was stopped when the iteration times achieve the predetermined times. Otherwise, the cyclic process as shown in Figure 6 will continuously proceed. Here, the iteration time was set as 50. The best individual in the last population was outputted as an approximate optimal solution. Additionally, then, the best individual was decoded into the parameter combination.

In this section, the partition of the training dataset and the testing dataset in GA-SVR is identical to the partition in LHS-SVR. Figure 7 shows the best fitness value and average fitness value corresponding to iteration times of GA-SVR. As illustrated in Figure 7, it can be observed that the convergence speed of GA-SVR is fast. In the first 10 iteration times, the average fitness value is approaching the best

fitness value state. The $C$, $\gamma$ and $\zeta$ of the best parameter combination ($R$ = 0.999961) are 29.6033, 7.3178 and 0.0651, respectively.

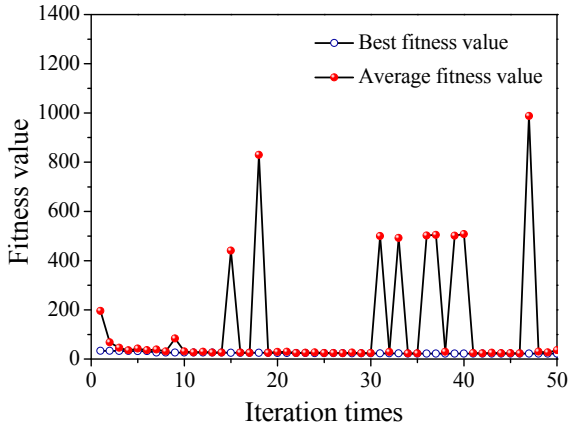


**Figure 7.** The relationships between the fitness values and the iteration times of GA-SVR.

## 4. Comparisons of the Mathematical Regression Model, ANN, LHS-SVR and GA-SVR of as-Forged Ti–10V–2Fe–3Al Alloy

### *4.1. The Existing Mathematical Regression Model and ANN of as-Forged Ti–10V–2Fe–3Al Alloy*

Quan et al. calculated a constitutive model at the strain of 0.5 for as-forged Ti–10V–2Fe–3Al alloy by the mathematical regression method, which just involves temperature and strain rate, as expressed by Equation (9) [20].

$$2.295 \times 10^9[\sinh(0.008065\sigma)]^{3.759} = \dot{\varepsilon}\exp(\frac{214.16}{RT}) \quad (9)$$

where σ is flow stress (MPa); $T$ is temperature (K); $R$ is the universal gas constant (8.31 J· mol$^{-1}$· K$^{-1}$); $\dot{\varepsilon}$ is the strain rate (s$^{-1}$).

Quan et al. established the ANN for the Ti–10V–2Fe–3Al alloy in [20].

### *4.2. Comparisons of Study Abilities of the ANN, LHS-SVR and GA-SVR*

The typical evaluation index of relative error (δ) expressed as Equation (10) was utilized to estimate the performance of these prediction models.

$$\delta\,(\%) = \frac{E_i - P_i}{E_i} \times 100\% \quad (10)$$

where $E$ is the sample of experimental stress-strain values; $P$ is the sample of predicted stress-strain values; $N$ is equal to the number of samples.

Another evaluation index of average absolute relative error (*AARE*) expressed as Equation (11), as an average number of the absolute value of δ-values, was adopted to further estimate the study abilities of these prediction models. Compared to δ-value, *AARE* can better reflect total prediction error.

$$AARE = \frac{1}{N}\sum_{i=1}^{N}\left|\frac{E_i - P_i}{E_i}\right| \quad (11)$$

where $E$ is the sample of experimental stress-strain values; $P$ is the sample of predicted stress-strain values; $N$ is equal to the number of samples.

Figure 8 shows the $R$-values and *AARE*-values between the training samples and fitted values of the LHS-SVR and GA-SVR of the Ti–10V–2Fe–3Al alloy. The $R$-values and *AARE*-values between the training samples and fitted values of ANN, LHS-SVR and GA-SVR are listed in Table 1. As shown

in Figure 8 and Table 1, it can be observed that the *R*-values between the training samples and fitted values of the LHS-SVR and GA-SVR model are larger than 0.9999, and the *AARE*-values of them are smaller than 0.402% of ANN. It can be summarized that LHS-SVR and GA-SVR can sufficiently and accurately learn the training samples. After comparisons of the *R*-values and the *AARE*-values of these models, it can be concluded that the study abilities of these models were shown as follows in ascending order: ANN < GA-SVR < LHS-SVR.

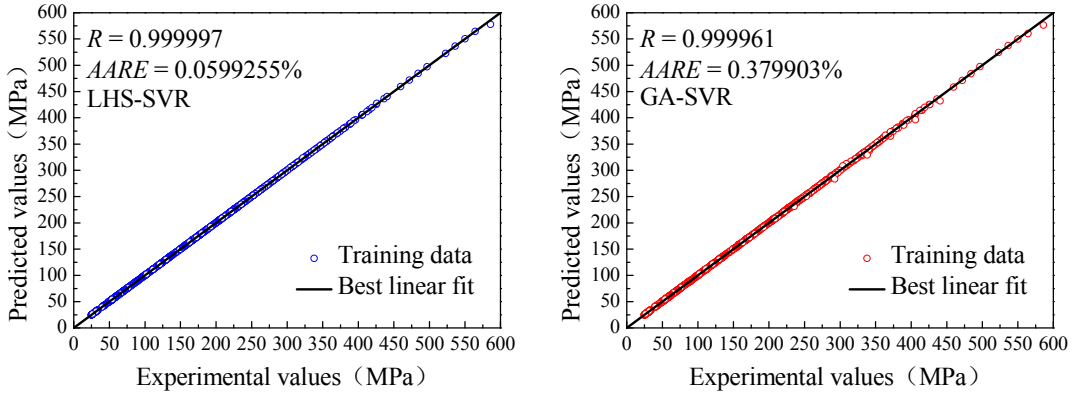


**Figure 8.** The *R*-values and *AARE*-values between the training samples and fitted values by (**a**) LHS-SVR and (**b**) GA-SVR of Ti–10V–2Fe–3Al alloy.

**Table 1.** *R*-values and *AARE*-values between the training samples and fitted values of ANN, LHS-SVR and GA-SVR of the Ti–10V–2Fe–3Al alloy.

| ***R*-Value** | | | ***AARE*-Value** | | |
|---|---|---|---|---|---|
| ANN | LHS-SVR | GA-SVR | ANN | LHS-SVR | GA-SVR |
| 0.9999 | 0.999997 | 0.999961 | 0.402% | 0.0599255% | 0.379903% |

### *4.3. Comparisons of the Generalization Abilities of the Mathematical Regression Model, ANN, LHS-SVR and GA-SVR*

Figure 9 shows the comparisons between the experimental flow stresses and testing flow stresses, which were predicted by the LHS-SVR and GA-SVR at different strain rates and temperatures. As shown in Figure 9, there is no singular point. The following work compared in detail the generalization abilities of LHS-SVR and GA-SVR.

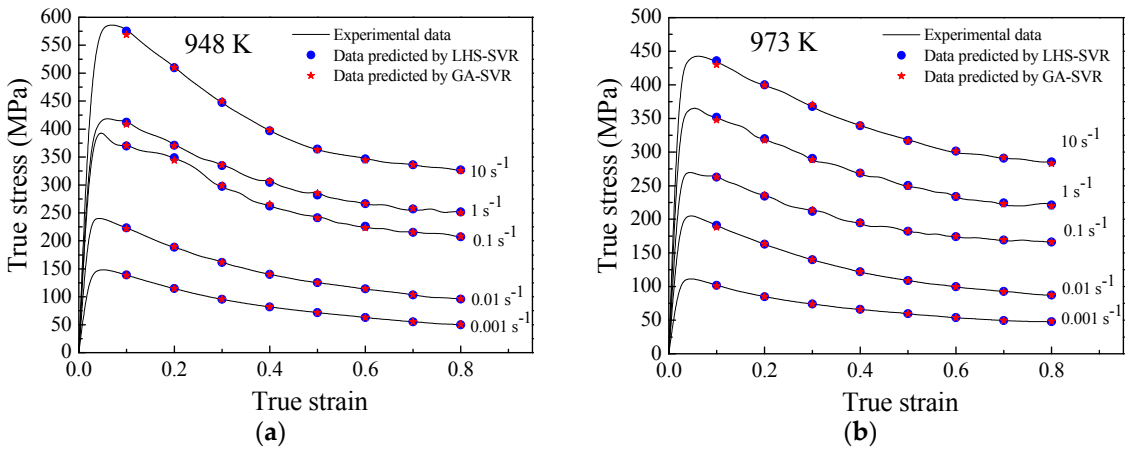


**Figure 9.** *Cont.*

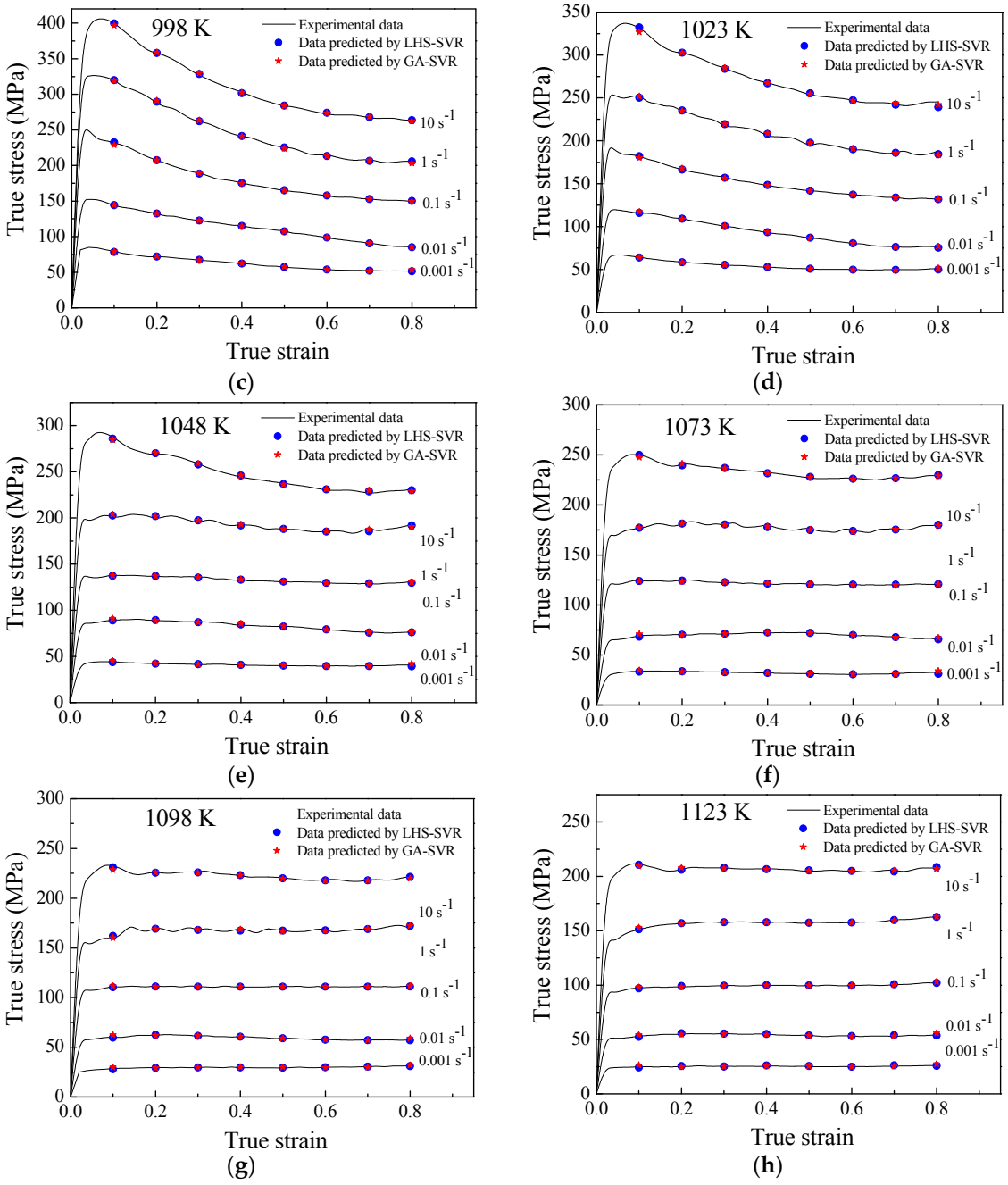


**Figure 9.** Comparisons between the trained flow stresses and the testing flow stresses predicted by LHS-SVR and GA-SVR at different strain rates and temperatures : (**a**) 948 K; (**b**) 973 K; (**c**) 998 K; (**d**) 1023 K; (**e**) 1048 K; (**f**) 1073 K; (**g**) 1098 K; (**h**) 1123 K.

Figure 10 shows the correlation between the experimental flow stresses and testing flow stresses of the LHS-SVR and GA-SVR model in the ($\alpha$ + $\beta$) and the $\beta$ phase, and the *R*-values of them are larger than 0.9998 at high accuracy levels.

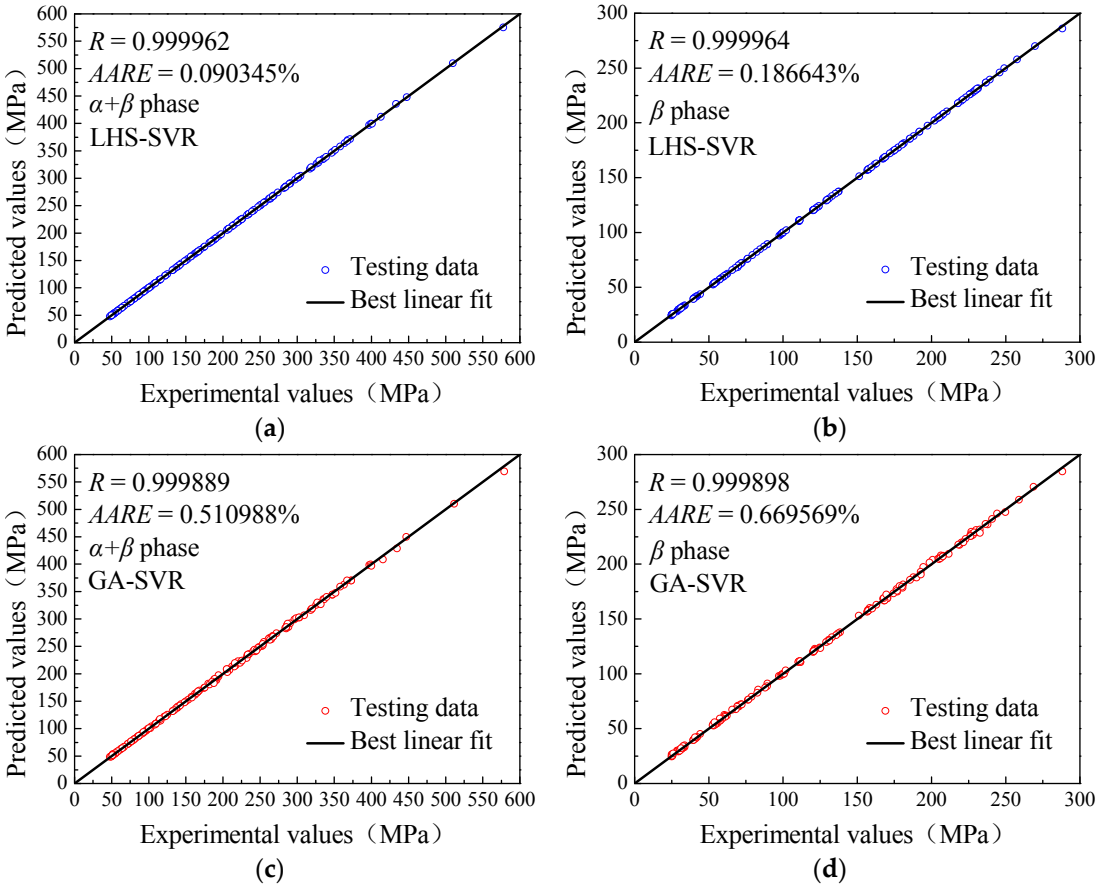


**Figure 10.** Correlation between the experimental flow stresses and the testing predictions of the LHS-SVR and GA-SVR in (α + β) and β phase: (**a**) predictions in (α + β) phase predicted by the LHS-SVR; (**b**) predictions in β phase predicted by the LHS-SVR; (**c**) predictions in (α + β) phase predicted by the GA-SVR; (**d**) predictions in β phase predicted by the GA-SVR.

Figure 11 shows the correlation between the experimental stresses and testing stresses of the LHS-SVR and GA-SVR model at the strain of 0.5, and the *R*-values of them are larger than 0.9999 at high accuracy levels. In order to show in detail the distribution and the relative frequency of $\delta$-values of the LHS-SVR and GA-SVR at the strain of 0.5, they were further analyzed by Gaussian distribution analysis. After Gaussian distribution analysis, the mean number of all of the relative errors (μ) and standard deviation (w) is obtained. The μ-value expressed by Equation (12) is the mean number of all of the relative errors. The standard deviation (w) expressed by Equation (13), as an evaluation index to measure the discrete degree of an individual in the dataset, was introduced to measure the distribution of the relative error (δ). Here, a small w indicates that most of δ-values are close to the μ-value, and vice versa. Additionally, a smaller μ-value indicates that more predicted stress data approach the experimental stress data.

$$\mu = \frac{1}{N}\sum_{i=1}^{N}\delta_i \tag{12}$$

$$w = \sqrt{\frac{1}{(N-1)}\sum_{i=1}^{N}(\delta_\iota - \mu)^2} \tag{13}$$

where δ is the sample of the relative error; μ is the average number of δ-values; N is equal to the number of samples.

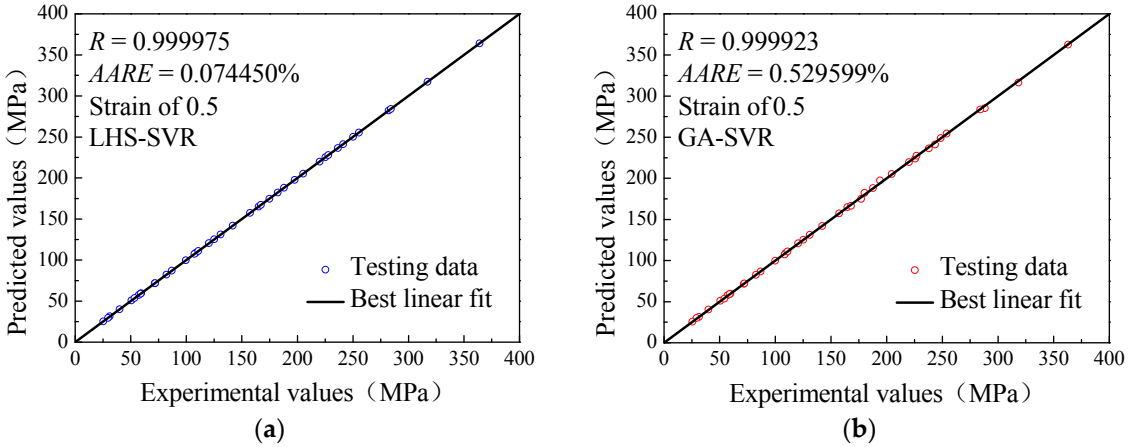


**Figure 11.** Correlation between the experimental flow stresses and the testing predictions by the (**a**) LHS-SVR and (**b**) GA-SVR at a strain of 0.5.

From Figure 12 and [20], it can be found that the δ-values acquired from the mathematical regression model, ANN, LHS-SVR and GA-SVR vary from −20%–20%, −3%–3%, −0.35%–0.05% and −3%–2%, respectively. Figure 12a,b shows the histogram of δ-values of LHS-SVR and GA-SVR, respectively, which show the relative frequency of each δ-level. The μ-value and w-value of the mathematical regression model, ANN, LHS-SVR and GA-SVR are 1.3146 and 8.2033, −0.1246 and 0.8745, 0.025 and 0.000407 and 0.00216 and 0.44195, respectively. It can be summarized that the generalization ability of the mathematical regression model is the worst, and the generalization abilities of LHS-SVR and GA-SVR are at higher levels.

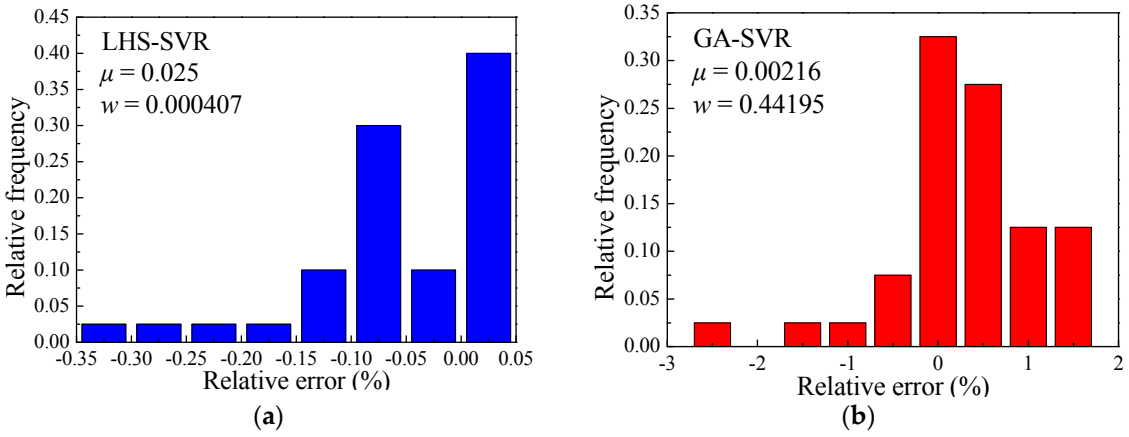


**Figure 12.** Distributions of the relative errors of the testing data by (**a**) LHS-SVR and (**b**) GA-SVR.

Table 2 exhibits the *R*-values and *AARE*-values of the testing dataset of the mathematical regression model, ANN, LHS-SVR and GA-SVR, so as to further compare the generalization abilities of these models. The *R*-values and *AARE*-values of the testing dataset at the strain of 0.5 of the mathematical regression model, ANN, LHS-SVR and GA-SVR are 0.9902 and 6.583%, 0.9998 and 0.572%, 0.999975 and 0.074450% and 0.999923 and 0.529599%, respectively. It can be observed that the LHS-SVR and GA-SVR have larger *R*-values and lower *AARE*-values, which indicate that the LHS-SVR and GA-SVR can accurately predict the highly non-linear flow behaviors. Compared to ANN, the globally-optimal solution can be obtained by using LHS-SVR and GA-SVR, and the computational processes of LHS-SVR and GA-SVR are robust and will avoid falling into local extreme values. For a certain dataset, the same network topology and training parameters of an ANN will obtain fluctuant accuracies in different

attempts. ANN can meet network topologies and training parameters well to achieve a higher accuracy level; however, these accurate results have poor reproducibility. The significant character of SVR is that an SVR with identical training parameters will maintain training accuracy and prediction accuracy at stable levels in different attempts for a certain dataset. The generalization abilities of these models were shown as follows in ascending order: the mathematical regression model < ANN < GA-SVR < LHS-SVR. The mathematical regression model cannot accurately track the hot flow behaviors, because the mathematical regression model has difficulty describing the complicated non-linear flow behaviors, which accompany phase transformation, WH, DRV and DRX in wide temperature and strain rate intervals. Worse still, the complicated calculation process of the mathematical regression model needs to be recomputed when some new experimental stress-strain data are involved. The LHS-SVR and GA-SVR do not need to establish the complicated mathematical models and the transformation mechanism of the micro structure. LHS-SVR and GA-SVR only need representative training samples from the study and then automatically adjust the three parameters $C$, $\gamma$ and $\zeta$ to obtain the most accurate SVR.

**Table 2.** The *R*-values and *AARE*-values of the testing dataset of the mathematical regression model, ANN, LHS-SVR and GA-SVR of the Ti–10V–2Fe–3Al alloy.

| Model \ Phase | *R*-Value | | | | *AARE*-Value | | | |
|---|---|---|---|---|---|---|---|---|
| | Regression Model | ANN | LHS-SVR | GA-SVR | Regression Model | ANN | LHS-SVR | GA-SVR |
| $\alpha + \beta$ | - | 0.99981 | 0.999962 | 0.999889 | - | 0.576% | 0.090345% | 0.510988% |
| $\beta$ | - | 0.99984 | 0.999964 | 0.999898 | - | 0.691% | 0.186643% | 0.669569% |
| Strain of 0.5 | 0.9902 | 0.9998 | 0.999975 | 0.999923 | 6.583% | 0.572% | 0.074450% | 0.529599% |

### *4.4. Comparisons of the Modelling Efficiencies of the Mathematical Regression Model, ANN, LHS-SVR and GA-SVR*

In Section 3.3, according to the preliminary search results where 1000 sample points were set in the intervals, $C \in [0, 100]$, $\gamma \in [0, 100]$, $\zeta \in [0, 100]$, only four *R*-values of the parameter combinations exceed 0.9999. In order to establish an accurate SVR model for as-forged Ti–10V–2Fe–3Al alloy, it is necessary to take much time and effort to manually adjust the three parameters one by one without using LHS-SVR. The intelligence algorithm LHS-SVR can automatically calculate the parameter combinations one by one in the search space to find the optimal value, which improves the computational efficiency to a certain extent.

Based on the selection, crossover and mutation operators, the GA-SVR can self-adaptively and dynamically adjust the processes of selection, crossover and mutation and rapidly generates the optimal parameter combination. These processes of GA-SVR greatly improve the computational efficiency compared to LHS-SVR. Table 3 illustrates the time in modelling an accurate model of the mathematical regression model, ANN, LHS-SVR and GA-SVR. ANN needs to try many network topologies and training parameters to obtain an accurate model, which will consume much time and effort. The LHS-SVR and GA-SVR only need representative training samples from the research and then automatically adjust the three parameters $C$, $\gamma$ and $\zeta$ to obtain the most accurate SVR. The modeling efficiencies of these models were shown as follows in ascending order: the mathematical regression model < ANN < LHS-SVR < GA-SVR.

**Table 3.** The time in modelling an accurate model of the mathematical regression model, ANN, LHS-SVR and GA-SVR.

| Model | Mathematical Regression Model | ANN | LHS-SVR | GA-SVR |
|---|---|---|---|---|
| The time in modelling an accurate model | More than 180 min | More than 60 min | About 20 min | About 10 min |

## 5. Applications of LHS-SVR in Material Computations

The flow stress data at temperatures of 948 K–1123 K and strain rates of 0.005 $s^{-1}$, 0.05 $s^{-1}$, 0.5 $s^{-1}$ and 5 $s^{-1}$ were predicted for as-forged Ti–10V–2Fe–3Al alloy by the LHS-SVR. Additionally, the predicted stress-strain curves at a temperature of 1123 K and strain rates of 0.005 $s^{-1}$, 0.05 $s^{-1}$, 0.5 $s^{-1}$ and 5 $s^{-1}$ are shown in Figure 13. The expanded stress-strain curves are conducive to accuracy improvement in the following fields.

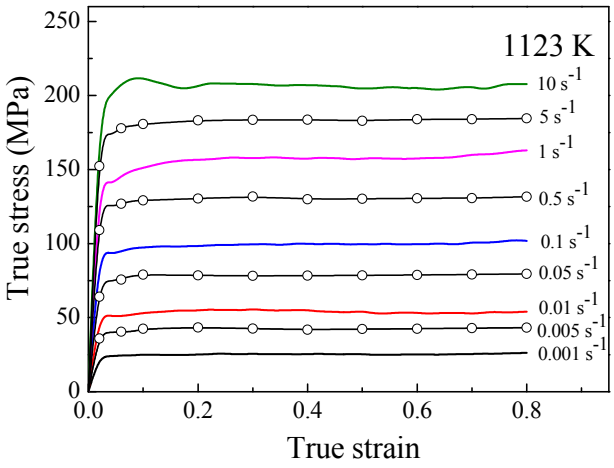


**Figure 13.** The true stress-strain curves of as-forged Ti–10V–2Fe–3Al alloy at a temperature of 1123 K and strain rates of 0.001 $s^{-1}$–10 $s^{-1}$, in which the solid curves are experimental data and the fitted curves by points are predicted data.

In this section, the impact of input stress-strain curves on simulation results was analyzed in a compression experiment by the FEM software DEFORM version 6.1 (Scientific Forming Technologies Corporation, Columbus, OH, USA). The simulation parameters were set based on the actual experiments. One half of the metal sample was simulated for the reason of geometric symmetry, so as to decrease the computing time. In the actual experiments, the top and bottom surfaces of the metal sample were coated with graphite lubricants to decrease friction between the sample and anvils; thereby, the friction type between the contact surfaces of the sample and dies was set as shear-type in DEFORM. In the simulations, the heat conduction and heat radiation among metal sample, dies and the ambient were ignored to simulate the isothermal experimental compression test. If the finite element software needs to invoke stress-strain data that are not beforehand inputted into the software, the software mainly calculates unknown stress-strain data by mathematical interpolation means. However, hot flow behaviors of materials at different conditions (such as different strain rates and temperatures) are highly non-linear and complicated. The mathematical interpolation method cannot correctly predict the data of materials and will obtain inaccurate simulation results. Therefore, in this section, the expanded stress-strain curves predicted by LHS-SVR were applied to enrich the stress data of the Ti–10V–2Fe–3Al alloy.

Two simulation schemes were designed to analyze the influences of input stress-strain curves on final simulation results. The entire initial conditions of the two simulation schemes are identical except for different input stress-strain curves. The compression tests were simulated at the temperature of 1123 K, the strain of 0.8 and a strain rate of 1 $s^{-1}$. The stress-strain curves at strain rates of 0.001–10 $s^{-1}$ and a temperature of 1123 K, which contain the predicted data, were applied to Scheme-A. The experimental stress-strain curves at strain rates of 0.001, 0.01, 0.1 and 10 $s^{-1}$ and a temperature of 1123 K were adopted by Scheme-B, so the stress-strain curve at a strain rate of 1 $s^{-1}$ and a temperature of 1123 K needs to be automatically interpolated by software.

Figure 14a displays the distribution of the effective stress of Scheme-A, which can be approximately divided into three districts. Figure 14b displays the distribution of the effective stress of Scheme-B, which can be similarly divided into three districts. However, there are large differences of the distributions of effective stresses between Scheme-B and Scheme-A, as well as the average effective stress.

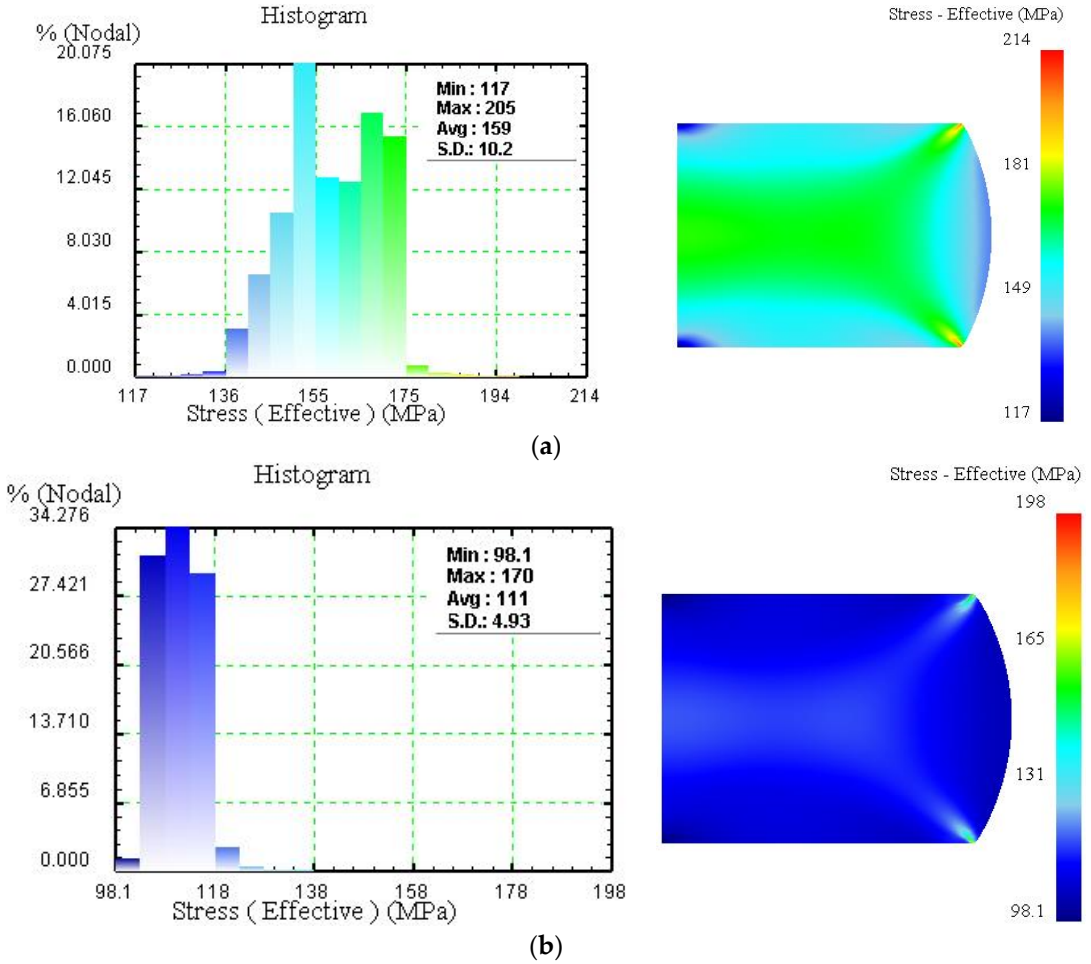


**Figure 14.** Distributions of the effective stress for (**a**) Scheme-A (**b**) and Scheme-B at the temperature of 1123 K, the strain of 0.8 and a strain rate of 1 $s^{-1}$.

In addition, as shown in Figure 15, the load curves corresponding to strokes of the top dies of these schemes show that the load curves of the top die of Scheme-A and the experimental values are very close. However, there are large differences of the top die loads between Scheme-B and the experimental values. The relative errors of the top die loads between Scheme-A and the experimental values are in the range of −4.6567945%–0.5856675%, whereas this errors between Scheme-B and the experimental values are in the range of 19.249696%–28.4626619%. It can be summarized that a large span of interpolation or insufficient stress-strain data will bring inaccurate simulation results. In addition, flow behaviors under different strain rates of a material are highly non-linear; thereby, calculating stress data by the interpolation method in FEM software is extremely inaccurate. In a precise manufacturing industry, the process requires accurate and sufficient material data, while the insufficient material data and inaccurate simulation results will cause great financial losses. LHS-SVR and GA-SVR can accurately predict the flow behaviors of materials, which can improve the related research fields, where stress-strain data play important roles, such as improving the accuracy of the finite element simulation result and improving processing maps.

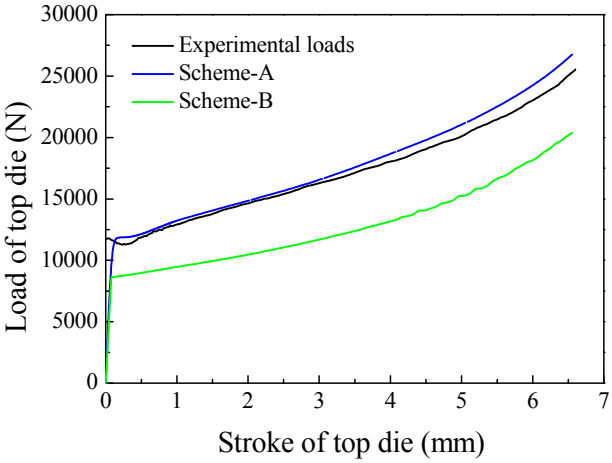


**Figure 15.** The relationship between the stroke and the load of the top die of experimental values, Scheme-A and Scheme-B.

## 6. Conclusions

The novel prediction models of LHS-SVR and GA-SVR were established to characterize the hot flow behaviors of as-forged Ti–10V–2Fe–3Al alloy according to the experimental stress-strain data. The following conclusions were derived from the current study:

(1) The study ability and generalization ability of SVR rely on the three parameters $C$, $\gamma$ and $\zeta$, especially the mutual impacts among them. An SVR with appropriate parameters $C$, $\gamma$ and $\zeta$ will accurately study the stress-strain curves and appropriately ignore some singular points of stress-strain data to accord with the overall trend of the stress-strain curves.

(2) The $R$-value and $AARE$-value between the training samples and fitted values of LHS-SVR and GA-SVR are 0.999997 and 0.0599255% and 0.999961 and 0.379903%, respectively, which show that LHS-SVR and GA-SVR can accurately learn the hot flow behaviors that accompany WH, DRV and DRX in wide temperature and strain rate intervals. The study abilities of these models were shown as follows in ascending order: ANN < GA-SVR < LHS-SVR.

(3) After the comparisons of the generalization abilities of these models at the strain of 0.5, LHS-SVR and GA-SVR have larger $R$-values and lower $AARE$-values of 0.999975 and 0.074450% and 0.999923 and 0.529599%, respectively, which indicate that LHS-SVR and GA-SVR can accurately predict the highly non-linear flow behaviors. The generalization abilities of these models were shown as follows in ascending order: the mathematical regression model < ANN < GA-SVR < LHS-SVR.

(4) The intelligence algorithm LHS-SVR can automatically calculate the parameter combinations in the search space to find the optimal value, which improves the computational efficiency compared to the mathematical regression model and ANN. Based on the selection, crossover and mutation operators, the GA-SVR can self-adaptively and dynamically search the optimal parameter combination, which greatly improves the computational efficiency compared to LHS-SVR. The modeling efficiencies of these models were shown as follows in ascending order: the mathematical regression model < ANN < LHS-SVR < GA-SVR.

(5) Hot flow behaviors of materials at different conditions (such as different strain rates and temperatures) are highly non-linear and complicated; therefore, calculating stresses by interpolation means in finite element software is inaccurate. The flow behaviors outside experimental conditions were predicted by the well-trained LHS-SVR, which enhance the simulation precision of the load-stroke curve and can further improve the related research fields where stress-strain data play important roles, such as improving the accuracy of finite element simulation results and improving processing maps.

**Acknowledgments:** This work was supported by the National Key Technologies R & D Program of China (2012ZX04010-081). The corresponding author appreciates the Chongqing Higher School Youth-Backbone Teacher Support Program.

**Author Contributions:** Guo-zheng Quan and Zhi-hua Zhang designed the experimental schemes; Le Zhang conducted the experiments; Zhi-hua Zhang and Le Zhang analyzed the experimental data; Qing Liu offered analysis tools and some valuable suggestion; Guo-zheng Quan and Zhi-hua Zhang wrote and revised this article.

**Conflicts of Interest:** The authors declare no conflict of interest.

## References

1. Li, L.; Ye, B.; Liu, S.; Hu, S.; Li, B. Inverse analysis of the stress–strain curve to determine the materials models of work hardening and dynamic recovery. *Mater. Sci. Eng. A* **2015**, *636*, 243–248. [CrossRef]
2. Quan, G.-Z.; Li, G.-S.; Chen, T.; Wang, Y.-X.; Zhang, Y.-W.; Zhou, J. Dynamic recrystallization kinetics of 42CrMo steel during compression at different temperatures and strain rates. *Mater. Sci. Eng. A* **2011**, *528*, 4643–4651. [CrossRef]
3. Quan, G.-Z.; Wang, Y.; Yu, C.-T.; Zhou, J. Hot workability characteristics of as-cast titanium alloy Ti–6Al–2Zr–1Mo–1V: A study using processing map. *Mater. Sci. Eng. A* **2013**, *564*, 46–56. [CrossRef]
4. Lin, Y.C.; Li, Q.-F.; Xia, Y.-C.; Li, L.-T. A phenomenological constitutive model for high temperature flow stress prediction of Al–Cu–Mg alloy. *Mater. Sci. Eng. A* **2012**, *534*, 654–662. [CrossRef]
5. Li, H.-Y.; Hu, J.-D.; Wei, D.-D.; Wang, X.-F.; Li, Y.-H. Artificial neural network and constitutive equations to predict the hot deformation behavior of modified 2.25Cr–1Mo steel. *Mater. Des.* **2012**, *42*, 192–197. [CrossRef]
6. Quan, G.-Z.; Lv, W.-Q.; Mao, Y.-P.; Zhang, Y.-W.; Zhou, J. Prediction of flow stress in a wide temperature range involving phase transformation for as-cast Ti–6Al–2Zr–1Mo–1V alloy by artificial neural network. *Mater. Des.* **2013**, *50*, 51–61. [CrossRef]
7. Jh, H. The effect heat treatment and carbon content on the work hardening characteristics of several steels. *Trans. ASM* **1944**, *32*, 123–133.
8. Guan, Z.; Ren, M.; Zhao, P.; Ma, P.; Wang, Q. Constitutive equations with varying parameters for superplastic flow behavior of Al–Zn–Mg–Zr alloy. *Mater. Des.* **2014**, *54*, 906–913. [CrossRef]
9. Fan, X.G.; Yang, H.; Gao, P.F. Prediction of constitutive behavior and microstructure evolution in hot deformation of Ta15 titanium alloy. *Mater. Des.* **2013**, *51*, 34–42. [CrossRef]
10. Sadough Vanini, S.A. Investigation of strain rate and temperature effects on mechanical behavior of functionally graded steels (FGSs) under hot compression. *Int. J. Phys. Sci.* **2012**, *7*, 5230–5238. [CrossRef]
11. Voyiadjis, G.Z.; Abed, F.H. Microstructural based models for bcc and fcc metals with temperature and strain rate dependency. *Mech. Mater.* **2005**, *37*, 355–378. [CrossRef]
12. Peng, W.; Zeng, W.; Wang, Q.; Yu, H. Comparative study on constitutive relationship of as-cast Ti60 titanium alloy during hot deformation based on arrhenius-type and artificial neural network models. *Mater. Des.* **2013**, *51*, 95–104. [CrossRef]
13. Xiao, J.; Li, D.S.; Li, X.Q.; Deng, T.S. Constitutive modeling and microstructure change of Ti–6Al–4V during the hot tensile deformation. *J. Alloy. Compd.* **2012**, *541*, 346–352. [CrossRef]
14. Sajadifar, S.V.; Yapici, G.G. Workability characteristics and mechanical behavior modeling of severely deformed pure titanium at high temperatures. *Mater. Des.* **2014**, *53*, 749–757. [CrossRef]
15. Kotkunde, N.; Deole, A.D.; Gupta, A.K.; Singh, S.K. Comparative study of constitutive modeling for Ti–6Al–4V alloy at low strain rates and elevated temperatures. *Mater. Des.* **2014**, *55*, 999–1005. [CrossRef]
16. Akbari, Z.; Mirzadeh, H.; Cabrera, J.-M. A simple constitutive model for predicting flow stress of medium carbon microalloyed steel during hot deformation. *Mater. Des.* **2015**, *77*, 126–131. [CrossRef]
17. Liu, J.; Zeng, W.; Lai, Y.; Jia, Z. Constitutive model of Ti17 titanium alloy with lamellar-type initial microstructure during hot deformation based on orthogonal analysis. *Mater. Sci. Eng. A* **2014**, *597*, 387–394. [CrossRef]
18. Quan, G.-Z.; Zhang, Z.-H.; Pan, J.; Xia, Y.-F. Modelling the hot flow behaviors of AZ80 alloy by BP-ANN and the applications in accuracy improvement of computations. *Mater. Res.* **2015**, *18*, 1331–1345. [CrossRef]
19. Haghdadi, N.; Zarei-Hanzaki, A.; Khalesian, A.R.; Abedi, H.R. Artificial neural network modeling to predict the hot deformation behavior of an A356 aluminum alloy. *Mater. Des.* **2013**, *49*, 386–391. [CrossRef]

20. Quan, G.-Z.; Zou, Z.-Y.; Wen, H.-R.; Pu, S.-A.; Lv, W.-Q. A characterization of hot flow behaviors involving different softening mechanisms by ANN for as-forged Ti–10V–2Fe–3Al alloy. *High. Temp. Mater. Process.* **2015**, *34*, 651–665.
21. Wang, H.; Li, E.; Li, G.Y. The least square support vector regression coupled with parallel sampling scheme metamodeling technique and application in sheet forming optimization. *Mater. Des.* **2009**, *30*, 1468–1479. [CrossRef]
22. Lou, Y.; Ke, C.; Li, L. Accurately predicting high temperature flow stress of AZ80 magnesium alloy with particle swarm optimization-based support vector regression. *Appl. Math. Inf. Sci.* **2013**, *7*, 1093–1102. [CrossRef]
23. Desu, R.K.; Guntuku, S.C.; Aditya, B.; Gupta, A.K. Support vector regression based flow stress prediction in austenitic stainless steel 304. *Procedia Mater. Sci.* **2014**, *6*, 368–375. [CrossRef]
24. Stein, M. Large sample properties of simulations using latin hypercube sampling. *Technometrics* **1987**, *29*, 143–151. [CrossRef]
25. Sakai, T.; Belyakov, A.; Kaibyshev, R.; Miura, H.; Jonas, J.J. Dynamic and post-dynamic recrystallization under hot, cold and severe plastic deformation conditions. *Prog. Mater. Sci.* **2014**, *60*, 130–207. [CrossRef]
26. Quan, G.-Z.; Kang, B.-S.; Ku, T.-W.; Song, W.-J. Identification for the optimal working parameters of Al–Zn–Mg–Cu alloy with the processing maps based on dmm. *Int. J. Adv. Manuf. Technol.* **2011**, *56*, 1069–1078. [CrossRef]
27. Keerthi, S.S.; Lin, C.-J. Asymptotic behaviors of support vector machines with gaussian kernel. *Neural Comput.* **2003**, *15*, 1667–1689. [CrossRef] [PubMed]
28. Chai, R.-X.; Guo, C.; Yu, L. Two flowing stress models for hot deformation of XC45 steel at high temperature. *Mater. Sci. Eng. A* **2012**, *534*, 101–110. [CrossRef]